THE 4TH INTERNATIONAL TOPICAL MEETING ON
NUCLEAR THERMAL HYDRAULICS, OPERATIONS AND SAFETY
April 6-8, 1994, Taipei, Taiwan

PREDICTIONS OF CRITICAL POWER BY COBRAG BASED ON A TWO-FLUID AND MULTI-FIELD MODEL

K.H. Chu and B.S. Shiralkar
GE Nuclear Energy (GE-NE)
175 Curtner Avenue
San Jose, California, USA
(408)-925-6087

ABSTRACT

Predictions of critical power by COBRAG based on a two-fluid, multi-field model were compared against the data collected at the ATLAS test facility at GE Nuclear Energy. Results of the comparisons are good with a relative percentage error generally less than 5%. The predicted trends in critical power versus some important physical parameters are also found to be in close agreement with experiments.

INTRODUCTION

Bundle critical power is one of the crucial parameters in optimizing the design of a BWR fuel bundle. A number of empirical correlations for critical quality based on bundle critical power measurements from full scale mockup tests under prototypical BWR operating conditions have been applied to BWR fuel bundle design and evaluation. However, these empirical correlations are restricted to the ranges of the experimental conditions and the design of the test bundles from which they are derived and extensive testing is required for new bundle designs. An alternate approach to predict the bundle critical power is by using a detailed subchannel analysis code. Such an approach has been adopted by several state-of-the art codes (e.g. COBRA-TF [1], THERMIT [2], MULTI [3] and FIDAS [4]) with different degrees of successes.

COBRAG is a detailed subchannel analysis code developed at GE Nuclear Energy with the main objective of predicting the critical power, the bundle pressure drop and the void distribution of the BWR fuel bundles. The two-phase flow is described by conservation equations derived from a two-fluid (e.g. liquid and vapor), multi-field (e.g. continuous, dispersed and multi-film) model. This model which allows films on different surfaces within a subchannel to have their own set of conservation equations proves to be crucial in predicting dryouts which occur on rods next to unheated surfaces(e.g. channel wall and water rod). The conservation equations are then coupled with other physical models such as inter-subchannel mixing, void drift, entrainment, deposition, shear and heat transfer models for closure. Critical power is controlled by the film dryout phenomenon which is modeled as a balance between evaporation, entrainment and deposition processes leading to a critical film thickness in an annular flow environment.

Qualification of COBRAG was performed in a systematic manner. Models simulating physical processes crucial in predicting bundle critical power such as entrainment and deposition, mixing and void drift, shear and heat transfer were first assessed by analyzing experiments designed to look at these processes separately. This was then followed by analysis of more complex tests with rod bundles and grid spacers to evaluate the integral performance of the models. Predictions from COBRAG were generally in close agreement with experimental data which demonstrates the adequacy of the models [5].

Critical power calculations were compared against experimental data to evaluate the performance of COBRAG in predicting bundle critical power. A large amount of critical power data have been collected at the ATLAS test facility at GE Nuclear Energy in San Jose where simulated BWR bundles of different designs have been tested at conditions within the range of normal BWR operation. A selected set of data from different bundle designs was used for comparison between the measured and calculated critical powers. Results of the comparisons are good with a relative percentage error for the majority of these predictions less than 5%. The predicted trends in critical power versus the bundle inlet mass flux and subcooling are also found to be in close agreement with experiments.

FORMULATION OF COBRAG

COBRAG extends the two-fluid model for two-phase flow to encompass multiple fields, which leads to a separate representation of the continuous and dispersed fields. In the annular flow regime, the liquid films, vapor and droplets are each represented by a set of conservation equations. In the bubbly flow regime, the sets of conservation equations for the films and droplets degenerate into one set to represent the continuous bulk liquid, and those for vapor to represent the bubbles.

The conventional flow centered subchannels (Figure 1) are adopted for COBRAG. In the annular flow regime, the different surfaces within a subchannel could have very different rates of heat generation and surface characteristics, and using a single field to represent an average film is not appropriate. To overcome this disadvantage, each film is modeled as a separate field. This also allows for more than one film segment around a fuel rod. A model simulating the wave spreading mechanism which tends to even out the film around the rod is included in COBRAG. However, differences in the azimuthal film thickness and flow will contribute to preferential dryout locations around the rod.

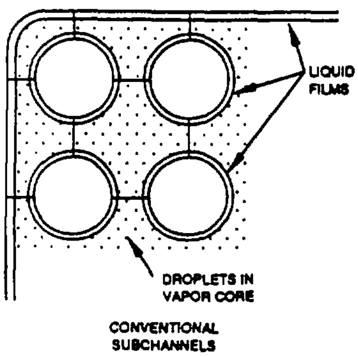

Figure 1. Flow Centered Subchannels

The conservation equations for each field are given as follows:

Mass Conservation Equation

$$\frac{\partial}{\partial t}(\alpha_k \varrho_k) = -\nabla \cdot (\alpha_k \varrho_k \vec{v}_k) + \Gamma_k + M_k + D_k$$

where

Γ_k : Mass source term due to evaporation or condensation

M_k : Mass source term due to turbulent mixing or film spreading

D_k : Mass source term due to entrainment or deposition

Momentum Conservation Equation

$$\frac{\partial}{\partial t}(\alpha_k \varrho_k \vec{v}_k) = -\nabla \cdot (\alpha_k \varrho_k \vec{v}_k \vec{v}_k) - \alpha_k \varrho_k \vec{g} - \alpha_k \nabla P - \vec{f}_{i,k} - \vec{f}_{w,k} + \vec{f}_{vd,k} + \Gamma_k \vec{v}_k^{\bullet} + \vec{B}_k + D_k \vec{v}_k^{\bullet}$$

where

$\vec{f}_{i,k}$: Interfacial force acting on phase k

$\vec{f}_{w,k}$: Force on phase k by the wall

$\vec{f}_{vd,k}$: Force acting on phase k due to void drift

$\Gamma_k \vec{v}_k^{\bullet}$: Momentum source term due to evaporation or condensation

$\vec{B}_k$: Momentum source term due to turbulent mixing or film spreading

$D_k \vec{v}_k^{\bullet}$: Momentum source term due to entrainment or deposition

Energy Conservation Equation

$$\frac{\partial}{\partial t}(\alpha_k \varrho_k h_k) = -\nabla \cdot (\alpha_k \varrho_k \vec{v}_k h_k) - \alpha_k \frac{\partial P}{\partial t} + q_{i,k} + q_{w,k} + \Gamma_k h_k^{\bullet} + E_k + D_k h_k^{\bullet}$$

where

$q_{i,k}$: Interfacial heat transfer from interface to phase k

$q_{w,k}$: Wall heat transfer from wall surface to phase k

$\Gamma_k h_k^*$: Energy source term due to evaporation or condensation

E_k : Energy source term due to turbulent mixing or film spreading

$D_k h_k^*$: Energy source term due to entrainment or deposition

This set of equations together with the following physical models can be solved numerically for pressure, and the velocities, volume fractions and enthalpies of each field.

PHYSICAL MODELS AND CONSTITUTIVE CORRELATIONS

To provide closure for the two-phase flow model, constitutive correlations for the following physical models were adopted for COBRAG.

Flow Regime Map

The flow regimes of a BWR bundle under typical BWR operating conditions ranges from bubbly flow near the inlet to annular dispersed flow at the exit. The flow regime map incorporated into COBRAG is summarized in Table 1.

Void Fraction	Flow Regime
0.0	Single Phase Liquid
$0.0 < \alpha_g < 0.3$	Bubbly Flow
$0.0 < \alpha_g < \alpha_t - 0.1$	Churn Flow
$\alpha_t - 0.1 < \alpha_g < \alpha_t$	Transition Regime
$\alpha_t < \alpha_g < 1.0$	Dispersed Annular Flow
1.0	Single Phase Vapor

Table 1. COBRAG Regime Map

The criterion for transition to dispersed annular flow is based on the condition when the film or the droplets can be lifted by the vapor flow. The vapor volume fraction at which the transition takes place is given by [6,7]:

$$\alpha_t = \left(1 + 4\frac{\rho_g}{\rho_\ell}\right)\frac{1}{c_o} - 4\frac{\rho_g}{\rho_\ell}$$

$$c_o = c_\infty(c_\infty - 1)\sqrt{\frac{\rho_g}{\rho_\ell}}$$

$$c_\infty = 1.393 - 0.015 \ln(\mathrm{Re})$$

Interfacial Shear and Heat Transfer

Models for interfacial shear and heat transfer are based on the extension of the two-fluid model used in the BWR version of TRAC. The interfacial shear is formulated based on the equivalence of the two-fluid and drift flux models at steady state, and the drift flux correlations developed from the void fraction data [8]. The model also includes a modification in subcooled boiling to account for the aggregation of vapor near the wall. The interfacial heat transfer for bubbles or droplets is modeled as heat transfer to a moving solid sphere, and for the film as heat transfer over a free surface [9,10]. The interfacial area for bubbles and droplets is given by sphere surface with radius determined from the critical Weber number, and for the film by the wall surface.

Deposition and Entrainment

Deposition is modeled as a mass transfer driven by the droplet concentration in the vapor core. The droplet deposition flux is given by:

$$G_{dep} = k \; f(C)$$

where k is the deposition coefficient and f (C) is a function of droplet concentration. The deposition coefficient k which can be viewed as a lateral drift velocity for the droplets [11], is correlated as:

$$k = A\frac{\mu_g}{\sigma D_h} \; f(x)$$

where A is an experimentally determined constant and f (x) is a function of flow quality.

Entrainment is modeled as liquid shearing off the film when the interfacial force overcome the surface tension. The droplet entrainment flux is correlated as [12]:

$$G_{ent} = A \; f(S_1, S_2)$$

where A is an experimentally determined constant and f (S_1,S_2) is a function two dimensionless parameters given by:

$$S_1 = \frac{\tau_\ell \delta}{\sigma}$$

$$S_2 = \frac{u_g \mu_\ell}{\sigma}$$

S_1 is results from balancing the interfacial force and the surface tension at the film surface and S_2 is a dimensionless vapor velocity to account for the effect of the vapor velocity.

Turbulent Mixing and Void Drift

Turbulent mixing is modeled as an equal volume exchange of two-phase mixtures among adjacent subchannels. The lateral mixing velocity is expressed as a product of a single phase mixing velocity and a two-phase multiplier:

$$j^* = j^*_{sp} \, \theta_{mix}$$

where the single phase mixing velocity is obtained from the transverse mixing flow rate per unit length correlated by Rogers and Rosehart [13] as:

$$W_{sp} = 0.005 \, D_h \, G \, Re^{-0.1}$$

and the two-phase multiplier by Rowe and Angle [14] as a function of mass flux and vapor volume fraction:

$$\theta_{mix} = 1 + f_1(\alpha) \, f_2(G)$$

In COBRAG, the formulation for the void drift phenomenon is based on the pressure gradient acting on the bubble resulting from a lateral velocity gradient between subchannels:

$$F_{vd} = f\left(\frac{\partial u}{\partial y}\right)$$

where the lateral force is formulated as a function of the lateral velocity gradient.

Film Based Dryout

The onset of the critical heat flux predicted by COBRAG is not based on empirical correlations but on the dryout of the of film instead. The multi-field approach which tracks the liquid film inventory for each rod surface provides a means for evaluating the dryout phenomenon directly. Physically, the condition for dryout corresponds to the situation where the heating surface is not completely covered by a liquid film. Since surface tension prevents an infinitely thin film, there exists a critical film thickness below which the film will break up to expose the heated surface. Models for critical film thickness under adiabatic conditions can be derived by balancing surface tension against interfacial shear at the film surface, which yields:

$$\delta_{crit} = \left[6 \, \frac{\sigma}{\varrho_\ell} \left(\frac{\mu_\ell}{\tau_i} \right) \right]^{\frac{1}{3}}$$

However, disturbances from the core flow tend to destablize the film by inducing waves on the film surface and result in a larger critical film thickness. Refinements to critical film thickness have been incorporated into COBRAG based on critical power data and can be expressed as:

$$\delta_{crit} = f\,(G)$$

where f is an experimentally determined function of mass flux.

Grid Spacer

Modeling of the interactions between grid spacer and two-phase flow is important to the performance of critical power prediction of a subchannel code. Developing a spacer model from first principles is difficult and may need more detailed information of the two-phase flow in its immediate vicinity like droplet distribution and velocity profiles within the subchannel. A semi-empirical approach has been applied to formulate the spacer grid model in COBRAG. The model analyzes the effects of the grid spacer on flow distribution (Figure 2) by focusing on the following mechanisms:

- Upstream film thinning
- Downstream turbulence enhancement
- Collection and runoff at spacer

The semi-empirical approach adopted by the spacer model requires that some key input parameters for the spacer model be adjusted for different spacers. However, only a few data points are needed for the adjustment and the adjusted input is then applied to all the other tests with the same spacer.

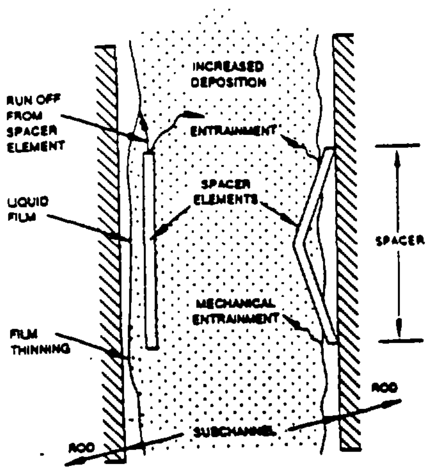

Figure 2. Spacer Interactions

CRITICAL POWER PREDICTION

A large amount of critical power data have been collected at the ATLAS test facility at GE Nuclear Energy at San Jose. Simulated BWR bundles of various lattices and using different grid spacers have been tested at conditions within the range of normal BWR operation and transients. To demonstrate the capability of COBRAG in predicting critical power over a wide range of physical parameters, several sets of critical power tests which covers different lattices, grid spacers, axial power profiles, pressures and inlet conditions were selected for comparison. Summary of the experimental conditions of the selected tests is listed in Table 2.

Lattice Type	8x8 to 10x10
Grid Spacer	Eggcrate, Ferrule, Unit Cell
Axial Pwr Profile	Cosine, Top and Bottom Peaked
Inlet Mass Flux	650–1850 kg/m^2/s
Inlet Subcooling	6–35 K
Pressure	5–9 MPa

Table 2. Experimental Conditions of the Selected Tests

Results are organized into groups and shown in Figures 3-8 to highlight the effect of each parameter. Very good overall comparisons have been achieved with a relative percentage error less than 5%. The accuracy of these predictions is comparable to the experimental uncertainty. Furthermore, the experimental trends in critical power versus pressure, inlet mass flux and subcooling, and axial power profile are are also accurately captured by COBRAG as shown in Figures 9-12.

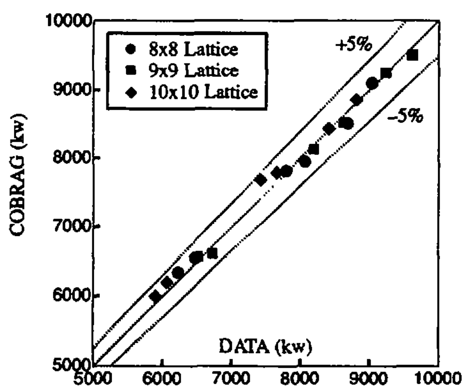

Figure 3. Critical Power Comparison for Different Lattices

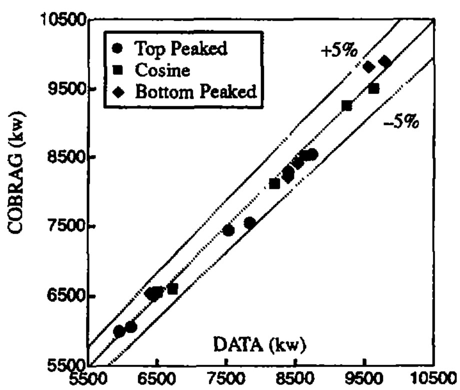

Figure 4. Critical Power Comparison for Different Axial Power Profiles

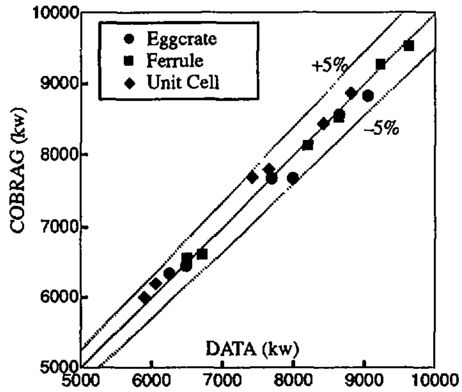

Figure 5. Critical Power Comparison for Different Spacers

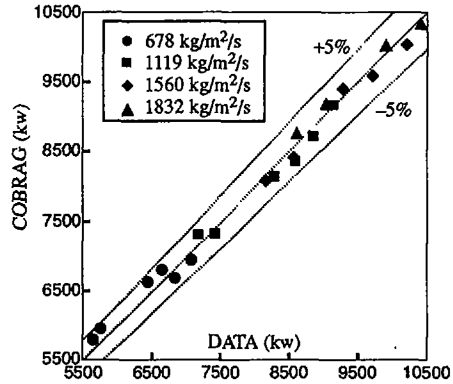

Figure 6. Critical Power Comparison at Different Inlet Mass Fluxes

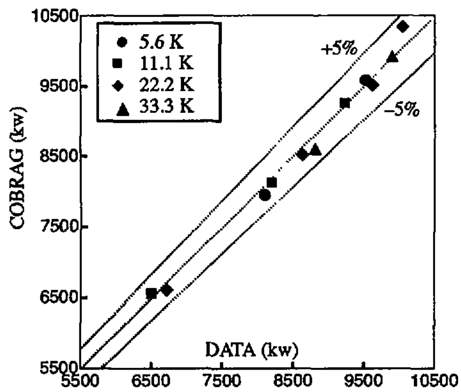

Figure 7. Critical Power Comparison at Different Subcoolings

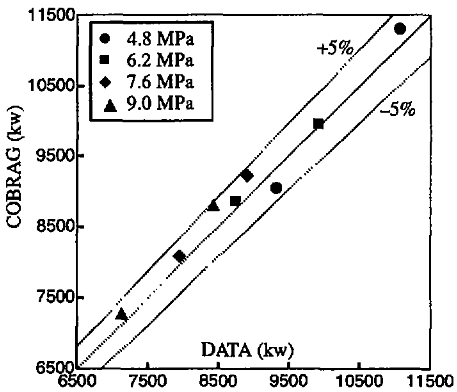

Figure 8. Critical Power Comparison at Different Pressures

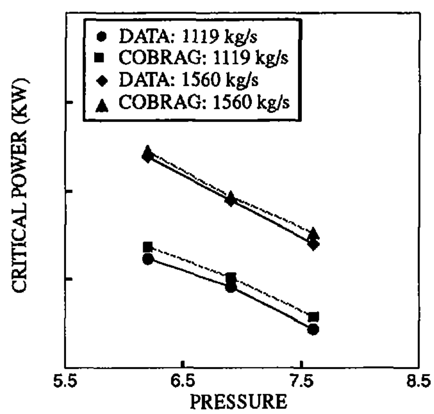

Figure 9. Critical Power Trends in Pressure

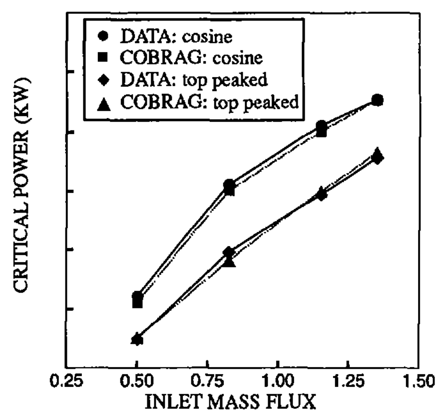

Figure 10. Critical Power Trends in Inlet Mass Flux

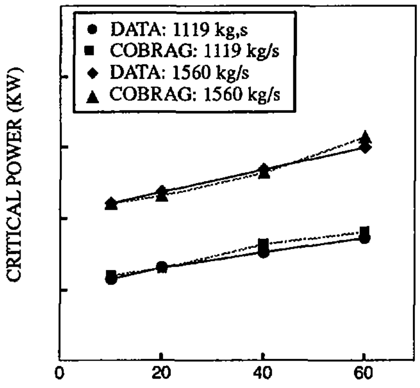

Figure 11. Critical Power Trends in Inlet Subcooling

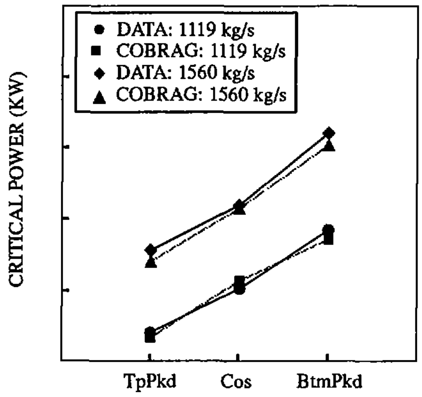

Figure 12. Critical Power Trends in Axial Power Profile

CONCLUSIONS

The capability of COBRAG in predicting the critical power of the BWR type fuel bundle was demonstrated by applying COBRAG to analyze the critical power data collected at the ATLAS test facility at GE Nuclear Energy. Data from different bundle designs and spacers under prototypical BWR operating was used for comparison. Predictions were found to be in close agreement with data. The maximum relative error is less than 5% and comparable to experimental uncertainty. Critical power trends with respect to several major physical parameters were also predicted accurately. These results demonstrate that the models in COBRAG is adequately formulated for the capability in performing critical power calculation.

NOMENCLATURE

C : Concentration
c_0 : Distribution parameter
D_h : Hydraulic diameter
F_{vd} : Force due to void drift
$\vec{g}$: Gravitational vector
G : Mass flux
h_k : Enthalpy of phase k
j : Volumetric flux
k : Deposition coefficient
P : Pressure
Re : Reynold number
t : time
u : Velocity
$\vec{v}_k$: Velocity of phase k
x : Flow quality

Greek

α_k : Volume fraction of phase k
δ : Film thickness
μ_k : Viscosity of phase k
ρ_k : Density of phase k
σ : Surface tension
θ_{mix} : Two-phase multiplier

Subscript

ℓ : Liquid
g : Vapor
sp : Single phase

REFERENCES

1. M.J. Thurwood, J.M. Kelly, T.E. Guidotti, R.J. Kohrt and K.R. Crowell, *COBRA / TRAC - A Thermal-Hydraulics Code for Transient Analysis of Nuclear Reactor Vessels and Primary Coolant Systems*, NUREG / CR-3046 (1983).
2. J.E. Kelly, S.P. Kao and M.S. Kazimi, *THERMIT-2: A Two-Fluid Model for Light Water Reactor Subchannel Transient Analysis*, MIT-EL-81-014 (1981).
3. T. Saito, *Multi-Fluid Modeling of Two-Phase Flow and Heat Transfer: Application to CHF Prediction for BWR*

Conditions, Ph.D. Thesis, Dept. of Nuclear Engg., U. Wisconsin, (1977).

4. S. Sugawara and Y. Miyamoto, *FIDAS: Detailed Subchannel Analysis Code Based on The Three-fluid and Three-field Model*, Nuclear Eng. Des. 120, (1990), pp. 146-161.

5. B.S. Shiralkar and K.H. Chu, *Recent Trends in Subchannel Analysis*, Subchannel Analysis in Nuclear Reactors, Edited by H. Ninokata and M. Aritomi, Atomic Energy Society of Japan, 1992.

6. M. Ishii, *One-Dimensional Drift-Flux Model and Constitutive Equations for Relative Motion Between Phases in Various Two-Phase Flow Regimes*, ANL-77-47, October 1977.

7. Y. Taitel, D. Borvea and A.E. Dukler, *Modeling Flow Pattern Transitions for Steady Upward Gas-Liquid Flow in Vertical Tubes*, AICHE Journal, No. 3, pp. 345-354, 1980.

8. J.G.M. Andersen, K.H. Chu, and J.C. Shaug, *BWR Refill-Reflood Program, Task 4.7 - Model Development, Basic Models for the BWR Version of TRAC*, NUREG/CR-2573, 1983.

9. R.J. Pryor, et al., *TRAC-P1A, An Advanced Best Estimate Computer Program for PWR LOCA Analysis*, Los Alamos Scientific Laboratory, NUREG/CRA-0665, LA-777-7S, May 1979.

10. J.G.M. Andersen and H. Abel-Larsen, *CORECOOL- Model Description of the Programme*, Dept. of Reactor Technology, Riso National Laboratory, Denmark, RISO-M-21380, November 1980.

11. A.W. Bennett, G.F. Hewitt, H.A. Kersey, and R.K.F. Keys, *Experiments on Burnout in a Uniformly Heated Tube at 1000 psia with Steam-Water Mixtures at the Tube Inlet*, AERE-R 5072, Harwell, England, 1965.

12. J. Wurtz, *An Experimental anf Theoretical Investigation of Annular Steam Water Flow in Tubes and Annuli at 30 ti 90 Bar*, RISO National Laboratory, Denmark, April 1978.

13. J.T. Rogers and R.G. Rosehart, *Mixing by Turbulent Interchange in Fuel Bundles, Correlations and Interferences*, ASME, 72-HT-53, 1972.

14. D.S. Rowe and C.W. Angle, *Cross Flow Mixing Between Parallel Flow Channels During Boiling*, BNWL-371, Battelle Northwest Laboratories, 1967.